Reduction of fluid forces for flow past side-by-side cylinders using downstream attached splitter plates

Ali Ahmed[1] · Shams Ul Islam[2] · Abdul Quayam Khan[3] · Abdul Wahid[3]

Abstract

A two-dimensional numerical simulation is performed to investigate the drag reduction and vortex shedding suppression behind three square cylinders with attached splitter plates in the downstream region at a low Reynolds number (Re = 150). Numerical calculations are carried out using the lattice Boltzmann method. The study is carried out for various values of gap spacing between the cylinders and different splitter plate lengths. The vortices are completely chaotic at very small spacing, as observed. The splitter plates are critical in suppressing shedding and reducing drag on the objects. The splitter plates with lengths greater than two fully control the jet interaction at low spacing values. There is maximum percentage reduction in $C_{D\mathrm{mean}}$ for small spacing and the selected largest splitter plate length. Furthermore, systematic investigation reveals that splitter plates significantly suppress the fluctuating lift in addition to drastically reducing the drag.

1 Introduction

Flow over bluff bodies have been studied for quite some time as a result of its wide scope of engineering applications such as buildings, pipelines, gas turbines, and many more. Despite the bluff body's (BB) simple geometry, it has a complex flow pattern on its rear. The flow separation at the front surface of BB causes a significant reduction in pressure in the back end of BB, which results in fluctuating forces acting on the body and causing flow-induced vibration. The aim of flow control is to minimize the resistance and power of such forces that act on the body. The use of better flow control can preserve energy and minimize body vibration. The methods used to control these forces are either active or passive control methods [1, 2]. Both of these methods control the shear layer and near wake instability. Among the two methods, the first

✉ Ali Ahmed
alihmd87@gmail.com

1 Department of Mathematics, University of Balochistan Quetta, Quetta, Pakistan

2 Department of Mathematics, COMSATS University Islamabad, Islamabad, Pakistan

3 Department of Mathematics, Balochistan University of Information Technology, Engineering and Management Science, Quetta, Pakistan

one required some external energy to control the flow (e.g., heating walls and synthetic materials, etc.), which made the method more complicated and costly. While in the second method, an additional device such as control cylinders, control plates, etc. is used to control the flow. As compared to the first method, the second one is easier and less costly. A control device such as a splitter plate can alter the vortex shedding which affect the F_D ($= \frac{\rho U_\infty^2 C_D D}{2}$, where ρ, U_∞, C_D, and D are the fluid density, uniform inflow velocity, drag coefficient and cylinder size, respectively). The splitter plate length is critical for delaying the shear layer toward the downstream end before it rolls up [3]. The splitter plate can either be attached to or detached from the BB. For an attached splitter plate, its size l/D (where l represents the splitter plate length) plays the key role in changing the flow structure. The spacing ratio (g/D) and splitter plate length (l/D) are both crucial factors in the scenario of a disconnected splitter plate.

To control the flow across the BB using an attached or detached splitter plate, numerous experimental and numerical studies have been done. Roshko [3] experimental work is one of the earliest to reveal that with the use of an attached splitter plate, the C_D decreases considerably. Wu and Shu [4] investigated the flow control for Reynolds number (Re = 100), using the Lattice Boltzmann method (LBM). They observed typical flow regimes and C_D reduction because of

the plate flipping motion. Okajima et al. [5] investigated experimentally the circular cylinder flow oscillation in a water tunnel in a free-oscillation test. They observed single and double excitation regions for aspect ratios of 5–10 and 14–21, respectively. Doolen [6] studied the flow through a square structure using a detached splitter plate. He observed that the structure of the wake changed with the use of plates, due to which a significant decline in the Strouhal number (St) and C_D occurred. Chauhan et al. [7] studied the flow over a square cylinder using an attached splitter plate. They observed that splitter plate modified the size of the wake and flow structure in the downstream. They further confirmed that drag and lift (C_L) coefficients decreases while increasing l/D. They also observed that after a particular value of l/D a secondary vortex arises on the verge of splitter plate. The C_D reduction on a cylinder with twin detached plates was numerically studied by Hwang and Yang [8]. They came to the conclusion that the upstream plate lowers the stagnation pressure while the downstream plate suppresses the vortex shedding, increasing base pressure. Vamsee et al. [9] numerically studied the splitter plate effect placed at both up and downstream for low Re. They noticed that the upstream regime's usage of splitter plates had greatly reduced the C_D. They also observed 27% reduction in C_D for detached and attached plate of length 1 and 2, respectively. Islam et al. [10] numerical observations of C_D reductions for downstream, upstream, and two-fold splitter plates were 62.2%, 13.3%, and 70.2%, respectively. Ali et al. [11] numerically studied the flow through a square structure using a splitter plate for a fixed Re = 150. They identified three flow regimes for different sizes of splitter plate. They observed the conversion of shear layers further downward before rolling up while increasing the splitter plate size for short splitter plate length ($0 < l/D < 1$). Cete and Unal [12] study of an attached splitter plate behind a circular cylinder noticed a continuous decrease in C_D while increasing the plate length from 0 to 2.

There have been a number of studies of splitter plates to control the flow through a single cylinder. However, very few studies have been conducted on the effect of splitter plates on flow over multiple structures. Kim and Durbin [13] studied the single splitter plate effect on flow through two cylinders at various locations. They found that the appropriate position of the plate caused the change in regime to occur from flopping to steady. Furqan and Mittal [14] investigated the flow across a pair of cylinders with flexible plates attached for a fixed Re = 100. They noticed that the early oscillations have a frequency that is much higher than the cylinder's natural frequency. Ahmed et al. [15] investigated the control cylinders' impact on the flow past three inline structures at Re = 160, while altering the control cylinder size (d/D) from 0.1 to 0.5 and g/D from 1 to 5D.

Many studies have been taken on flow past multiple cylinders arranged side-by-side without using control methods.

Zhan and Zhou [16] experimentally studied the effect of uneven g/D value on flow past three structures for Re = 150–2000. They observed symmetric flow at $g/D = 1.5$. They also discovered that a small change in spacing caused the flow pattern to shift from symmetric to asymmetric. Virahsawmy et al. [17] numerically studied the unstable flows behind three circular cylinders for Re = 300, at (g_1/D, g_2/D) (where g_1 is the distance from the lower to the middle cylinders and g_2 is the distance from the middle to the upper cylinder) = (1.5, 1.6). They discovered that the downstream reformation of wake flow changes and becomes unstable. Junkao et al. [18] studied the flow across three cylinders at low Re. They observed that essential factors in the production of vortices are the strength and phase of gap flow. Kang [19] studied the flow across three structures for $g/D < 5$ at Re = 100. He discovered that at small spacing, the $C_{D\text{mean}}$ value of the outer cylinders is greater than the value of the single cylinder. Sumner et al. [20] investigated the flow behind two and three cylinders for Re = 500–3000 and $g/D = 1$–6. They observed symmetric and asymmetric biased flow regimes for three structures at $g/D = 1.25$. The studies of flow past three structures were also carried out by Rahman et al. [21], Zheng and Alam [22], Islam et al. [23], Inoue and Suzuki [24], Kumada et al. [25] and Guillaume and LaRue [26].

In fluid, the studies have also been taken on for different dynamic models describing many real-world aspects. A number of researchers have been working in this field. Here, we will discuss a few of them. Zafar et al. [27] studied the dynamic behaviour of tuberculosis using a fractional mathematical model. In order to investigate the COVID-19 model's existence, HU stability, and computational outcomes, Khan et al. [28] used five classes of population as their basis. They used a numerical method to analyze the data from the literature and obtained intriguing findings for various frictional ordering. Zafar et al. [29] investigated the clinical correlations and dynamic behaviour of tuberculosis using a fractional mathematical model that included Atangana-Baleanu.

From the above discussion, it is clear that although there have been numerous studies on the flow past three side-by-side cylinders; no research has been conducted on the proposed problem. Our main aim is to increase understanding of flow across a series of square cylinders with attached splitter plates at downstream in a side-by-side arrangement, for a fixed Re = 150. Another important subject on the agenda is the reduction of fluid forces and vortex shedding, especially at low g/D values.

The organization of the remaining section is as follows: Sect. 2 consists of a description of the problem, its initial conditions, and boundary conditions. Section 3 consists of numerical method details. Section 4 consists of computational domains, grid independence, and code validation.

Sections [5] and [6] consist of results, discussion, and conclusions, respectively.

2 Problem description

The proposed problem's geometry is shown in Fig. [1]. A two-dimensional (2D) numerical study is organized under the effect of *g/D* between the cylinders and the splitter plate size *l/D* attached to the cylinder in the downstream region. The study is conducted for a constant Reynolds number (Re = 150), with spacing ranging from 0.5 to 4, and splitter plate length ranging from 1 to 5. The length and height of the channel are denoted by L_x and L_y, respectively. The upstream, downstream, and vertical distances of the channel are $L_u = 8D$, $L_d = 25D$ and $L_y = 11D$, respectively. These numbers were chosen after careful consideration in order to minimize the impact of the inlet and outlet boundary conditions. At the channel's inlet, the uniform inflow velocity is applied, whereas the convective boundary condition is used at the channel's exit [30]. No-slip boundary conditions are employed on the surface of cylinders, while periodic boundary conditions are utilized at the top and bottom of the channel. [31]. For the calculation of fluid forces, the moment exchange method is used [32]. In Fig. [1], C1, C2, and C3 represent the lower, middle, and upper cylinders, respectively.
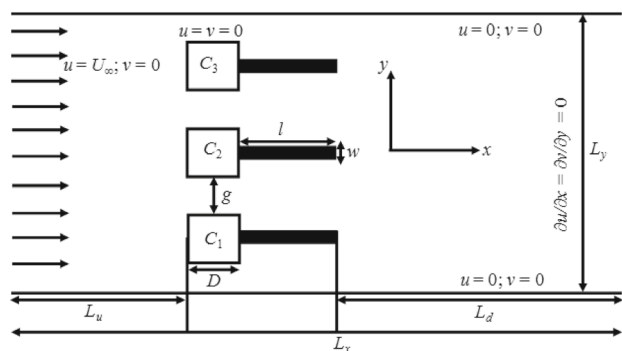
The governing equations for the flow of incompressible fluids are as follows:

Momentum equation

$$\partial_t \boldsymbol{u} + (\boldsymbol{u} \cdot \nabla)\boldsymbol{u} = \frac{1}{\rho}\nabla p(x, y; t) + \nu\nabla^2\boldsymbol{u} \qquad (1)$$

and continuity equation

$$\nabla \cdot \boldsymbol{u} = 0, \qquad (2)$$

Fig. 1 The geometry of proposed problem of flow past three cylinders with attached splitter plates in an unconfined channel

Subject to suitable boundary conditions. In Eq. [(1)] x and y are the streamwise and transverse directions. The macroscopic velocities are indicated by $\boldsymbol{u} = (u, v)$ in the equations above. The fluid density, pressure field, and kinematic viscosity are each represented by the letters ρ, p, and v, respectively. $\nabla = (\partial x, \partial y)$ is the nabla operator is.

The definitions of the drag coefficient (C_D) and lift coefficient (C_L) are

$$C_D = 2F_D/\rho U_\infty^2 D, \qquad (3)$$

$$C_L = 2F_L/\rho U_\infty^2 D, \qquad (4)$$

where F_D, F_L, U_∞, ρ and D are the drag force, lift force, uniform inflow velocity, fluid density, and cylinder side length, respectively.

The Reynolds number and Strouhal number—each of which are specified by Eqs. [(5)] and [(6)], are the non-dimensional parameters that are utilized.

$$\text{Re} = U_\infty D/\upsilon, \qquad (5)$$

$$St = f D/U_\infty, \qquad (6)$$

where υ and f are the kinematic viscosity and vortex shedding frequency, respectively.

3 Lattice Boltzmann method (LBM)

A 2D LBM code was developed in this study for the flow behind three square cylinders with attached splitter plates at $(g/D, l/D) = (0.5–4, 1–5)$ for a constant Re = 150. The 2D is used because of its low Reynolds number.

LBM is the latest numerical technique used to solve fluid dynamics problems. It was developed by Frisch et al. [33]. This method serves as a good alternative approach for modeling physical phenomena in fluid flow. The LBM is an approach to discrete kinetic theory that includes a mesoscale description of the fluid's microstructure compared to traditional numerical methods including the spectral, element method, FDM, FEM, and FVM, which are based on the discretization of the macroscopic continuum equations. Boltzmann's main idea is to bridge the gap between macro- and micro-scales by looking at the behaviour of a group of particles rather than individual particles. A distribution function represents the property of a collection of particles. This function serves as a representative of the collection of particles. The scale is known as the mesoscale.

Here, we will provide a brief summary of the method. In this study, the p_2q_9 (where p is space dimension and q is the particle number) model is applied. Each computing node in
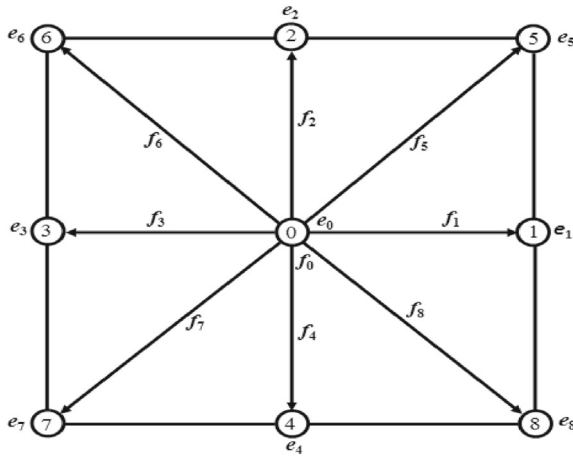
Fig. 2 LBM lattice velocities on square structure

this model is composed of nine particles: one rest particle ($i = 0$) and eight moving particles ($i = 1$–8) make up each computing node (Fig. 2)).

The equation for density evolution is given by;

$$f_i(\boldsymbol{x} + e_i, t + 1) = f_i(\boldsymbol{x}, t) - \left[f_i(\boldsymbol{x}, t) - f_i^{(\mathrm{eq})}(\boldsymbol{x}, t) \right]/\tau \tag{7}$$

where f_i and $f_i^{(\mathrm{eq})}$ are particle distribution function and corresponding equilibrium distribution function, $\boldsymbol{e_i}$ are the velocity directions, t, $\boldsymbol{x}$ and τ are the dimensionless time, the particles position, and the single relaxation time, respectively.

The corresponding equilibrium distribution function is:

$$f_i^{(\mathrm{eq})} = \rho \omega_i \left(1 + 3(\boldsymbol{e_i} \cdot \boldsymbol{u}) + 4.5(\boldsymbol{e_i} \cdot \boldsymbol{u})^2 - 1.5\boldsymbol{u}^2 \right) \tag{8}$$

Here ρ, $\boldsymbol{u}$ and ω_i are the fluid density, $\boldsymbol{u}$ is the instantaneous velocity, and ω_i is the corresponding weight functions ($\omega_i = 0$ for $i = 0$, $\omega_i = 1/9$ for $i = 1$–4, and $\omega_i = 1/36$ for $i = 5$–8).

Equation (7) can be solved using two steps: collision, which makes use of a BGK operator [20, 33], and propagation. These actions can be summed up as:

$$\text{Collision}: f_i^{(\mathrm{new})}(\boldsymbol{x}, t) = f_i(\boldsymbol{x}, t) - \left[f_i(\boldsymbol{x}, t) - f_i^{(\mathrm{eq})}(\boldsymbol{x}, t) \right]/\tau \tag{9}$$

$$\text{Streaming}: f_i(\boldsymbol{x} + \boldsymbol{e_i}, t + 1) = f_i^{(\mathrm{new})}(\boldsymbol{x}, t). \tag{10}$$

Following the streaming stage, boundary conditions are used, and the problem is then iteratively solved. At each computing node, the densities and velocities are determined using Eqs. (11) and (12).

$$\rho = \sum_i f_i \tag{11}$$

Table 1 Cylinder size effect on integral parameter at Re = 150

D	$C_{D\mathrm{mean}}$	St
10	1.52 (8%)	0.162 (7%)
20	1.44 (2%)	0.156 (3%)
30	1.41	0.152

$$\rho \boldsymbol{u} = \sum_i f_i e_i \tag{12}$$

The equation of state ($p = \rho c_s^2$, where c_s is the speed of sound and its value is $1/\sqrt{3}$) is used to calculate pressure.

4 Computational domain study and code validation

4.1 Grid independence study

The grid independence analysis for flow across an isolated cylinder is shown in Table 1. The error in brackets is calculated using a cylinder size of $D = 30$. The data shows that by changing the value of D from 20 to 30, the maximum difference in $C_{D\mathrm{mean}}$ and St are 2% and 3%, respectively. Based on these results, we choose $D = 20$ for the simulations of the proposed problem.

4.2 Computational domain study

The flow characteristics around the BB are strongly affected by the computational size. The vortex shedding procedure changes, when there is a small change in computation domain size, resulting in a change in physical parameters. We calculated the $C_{D\mathrm{mean}}$ and St using varied L_u, L_d, and L_y, values in order to select an appropriate computational domain. We noticed a slight difference in the results (Ref. Table 2). So From Table 2, we can consider any case. For the given problem, we will use $L_u = 8D$; $L_d = 25D$, and $L_y = 11D$.

The computational domain for the codes developed for the proposed is given in Tables 3 and 4.

4.3 Code validation

The validation of the code is done using the flow past a single cylinder for the selected Re. The $C_{D\mathrm{mean}}$ and St are the only parameters used for code validation. Table 5 shows the experimental data of Okajima [35] and Sohankar et al. [36] as well as the numerical data of Gera et al. [37]. The results reveal that $C_{D\mathrm{mean}}$ solutions agree with Okajima's [35] and Gera et al.'s [37], experimental and numerical data. The St has shown good agreement with Sohankar et al.'s [36] experimental findings.

Table 2 Computational domain effect at $g/D = 1$ and $l/D = 5$

L_u	L_d	L_y	C_{Dmean1}	C_{Dmean2}	C_{Dmean3}	St1	St2	St3
$8D$	$25D$	$11D$	2.0509	1.9770	2.0509	0.1543	0.1127	0.1543
			1%	0.7%	1%	0%	0%	0%
$8D$	$40D$	$11D$	2.0308	1.9762	2.0309	0.1543	0.1127	0.1543
$8D$	$25D$	$11D$	2.0509	1.9770	2.0509	0.1543	0.1127	0.1543
			1.97%	1.840%	(1.97%)	1.426%	(2.307%)	(1.426%)
$12D$	$25D$	$11D$	2.0104	1.9407	2.0106	0.1521	0.1101	0.1521
$8D$	$25D$	$11D$	2.1262	2.0438	2.1269	0.1586	0.1161	0.1586
			3.541%	(3.268%)	3.573%	2.711%	2.928%	2.711%
$8D$	$25D$	$14D$	2.0509	1.9770	2.0509	0.1543	0.1127	0.1543

Table 3 Computational domain without splitter plates

g/D	$L_x \times L_y$
0.5	681×261
1	681×281
2	681×321
3	681×361
4	681×401

Table 5 Comparison of present and previous results

|	C_{Dmean}	St
Present	1.44	0.157
Okajima [33]	1.45	0.141
Sohankar et al. [34]	–	0.156
Gera et al. [20]	1.41	0.141

5 Results and discussion

In this study, we examine how spacing ($0.5 \leq g/D \leq 4$) and splitter plates of size ($1 \leq l/D \leq 5$) affect hydrodynamic parameters such as flow regimes, time histories of force coefficients, power spectrum analysis of C_L, and instantaneous vorticity contour visualization representation (IVCVR) for flow past three square cylinders at a fixed Re = 150. The splitter plates are attached to the middle of the rear side of the cylinders. During the whole investigation, different flow regimes have been observed that are named according to vortex generation mechanisms and force variation. The Calculation of force statistics, C_{Dmean}, C_{Drms}, C_{Lrms} and St is also discussed. Here, we used C_{Dmean1}, C_{Dmean2}, C_{Dmean3}, C_{Drms1}, C_{Drms2}, C_{Drms3}, C_{Lrms1}, C_{Lrms2}, C_{Lrms3}, St1, St2, St3 for mean drag coefficients, root-mean-square values of drag coefficients, lift coefficients, and St of C_1, C_2, and C_3, respectively.
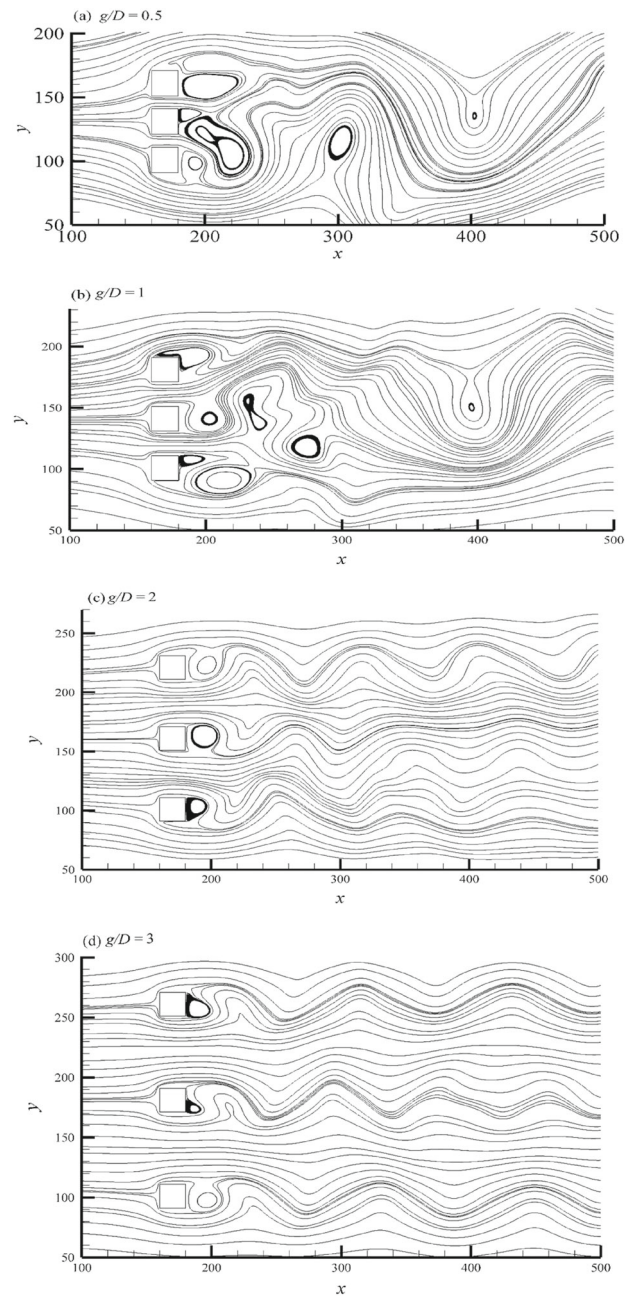
Table 4 Computational domain with splitter plates

g/D	l/D	$L_x \times L_y$	g/D	l/D	$L_x \times L_y$
0.5	1	701×261		4	761×321
	2	721×261		5	781×321
	3	741×261	3	1	701×361
	4	761×261		2	721×361
	5	781×261		3	741×361
1	1	701×281		4	761×361
	2	721×281		5	781×361
	3	741×281	4	1	701×401
	4	761×281		2	721×361
	5	781×281		3	741×361
2	1	701×321		4	761×361
	2	721×321		5	781×361
	3	741×321			
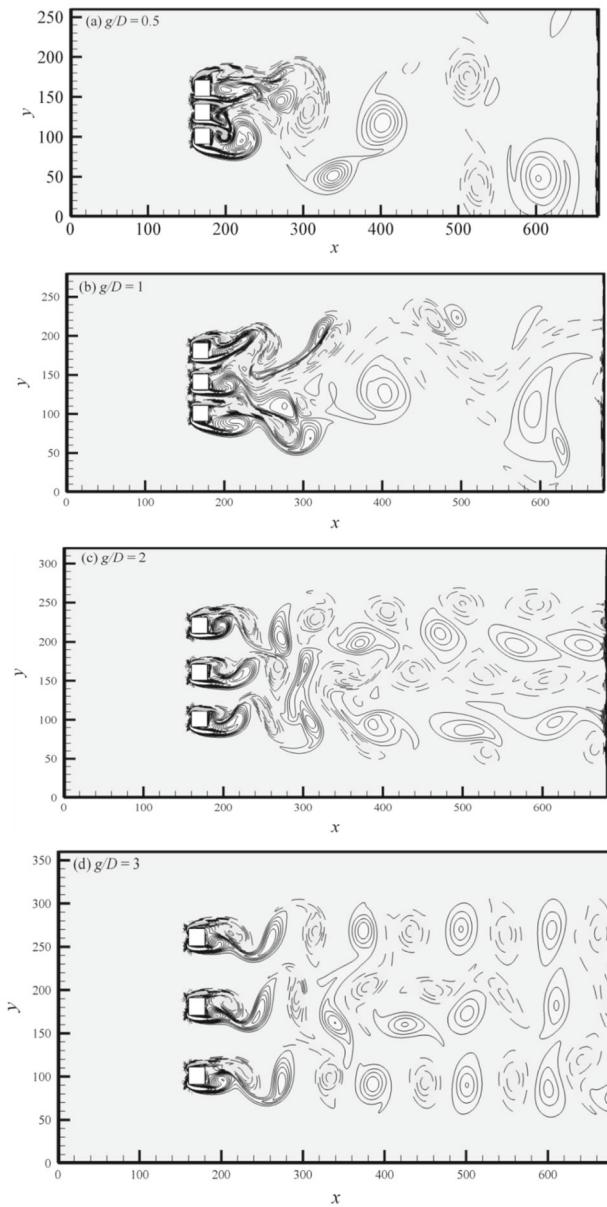
Fig. 3 (**a–d**) Vorticity contour visualization at different *g/D* values

Fig. 4 (**a–d**) Streamline visualization of flow past three cylinders at different *g/D* values

5.1 Flow features without splitter plates

The present computations show that flow across three side-by-side cylinders at a low Re considerably depends on the *g/D* between the cylinders. Figures 3a–d and 4a–d show the visualizations of instantaneous vorticity contours and streamlines, respectively. The corresponding time variation of the forces is presented in Fig. 5a–d. The spectrum analysis of C_L further confirms the vortex patterns behind each structure in Fig. 6a–d. The figures show two various flow regimes observed at various *g/D* values at Re = 150: flip-flopping or irregular (Fig. 3a, b) and modulation-synchronized flow regimes (Fig. 3c, d). This confirms that the pattern of the

flow strongly depends on the *g/D* and agrees well with available experimental studies Kumada et al. [25]; Guillaume and LaRue [26] at fairly high Re.

At *g/D* = 0.5 (Fig. 3a), the flow is remarkably unsteady and no longer periodic. It is noted that the two gap flows meaningfully affect the near downstream wakes, leading to wide and narrow wakes behind the middle and outer cylinders, respectively. The irregularity is further highlighted in the streamline visualization presented in Fig. 4a. As a result, the C_D of the outer structures is considerably lower than

Fig. 5 (**a**–**h**) Time variation of forces at different *g/D* values
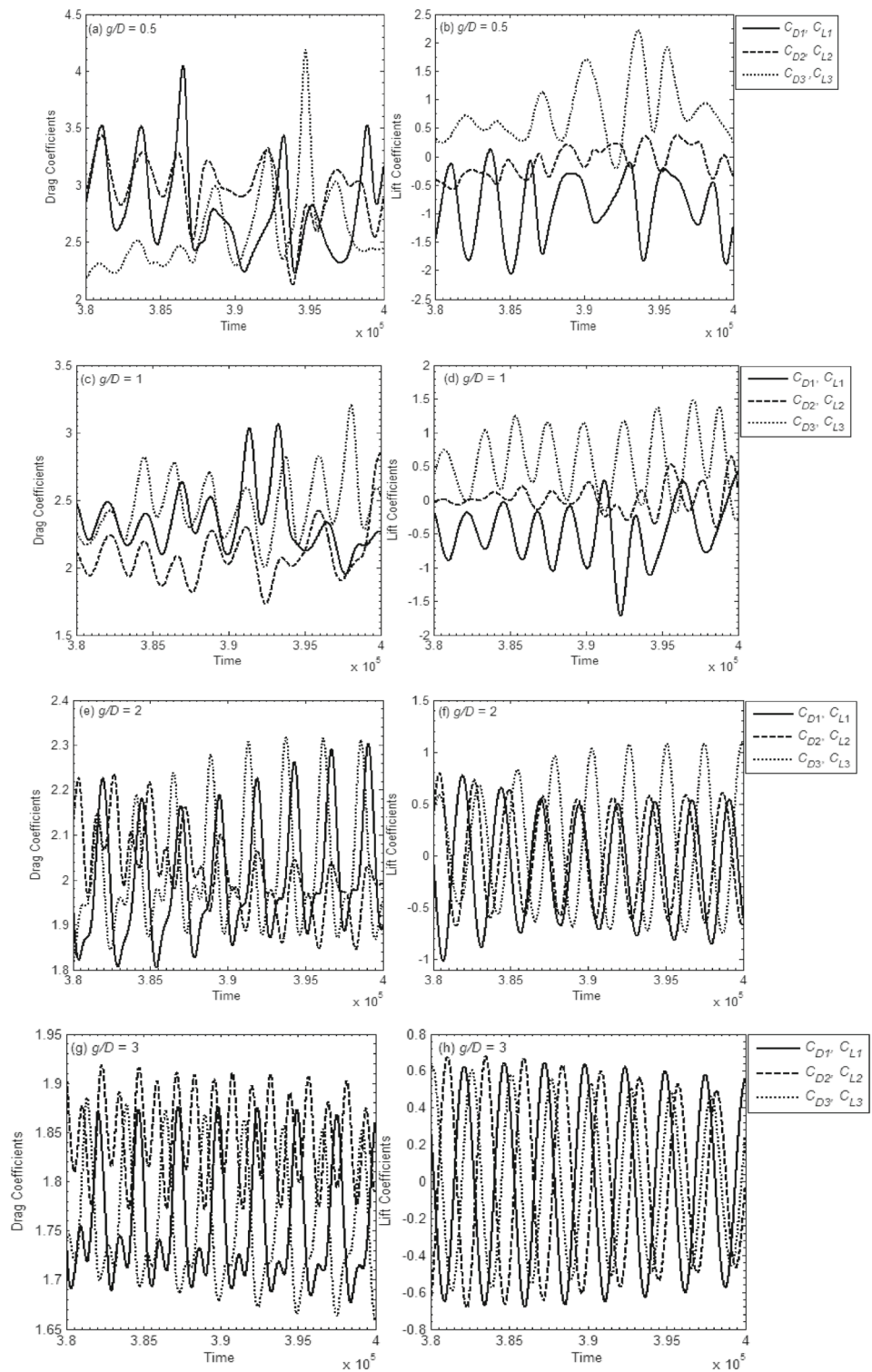
the C_D of the middle cylinder (Fig. 7a). The time variation of forces shown in Fig. 5a–f confirms the irregular variation of wakes behind the cylinders. Due to these features, the flow regime is called the flip-flopping flow regime. Such flow regimes are also observed experimentally by Guillaume and LaRue [26] for high Re and numerically by Kang [19] for low

Re. The power spectra for this flow regime demonstrate that various dominating frequencies are spread unevenly over a wide range (Fig. 6a–c).

At $g/D = 1$ (Fig. 3b), the flow is still unsteady and no longer periodic. As compared to $g/D = 0.5$, the C_D of the outer cylinders is considerably higher than the drag
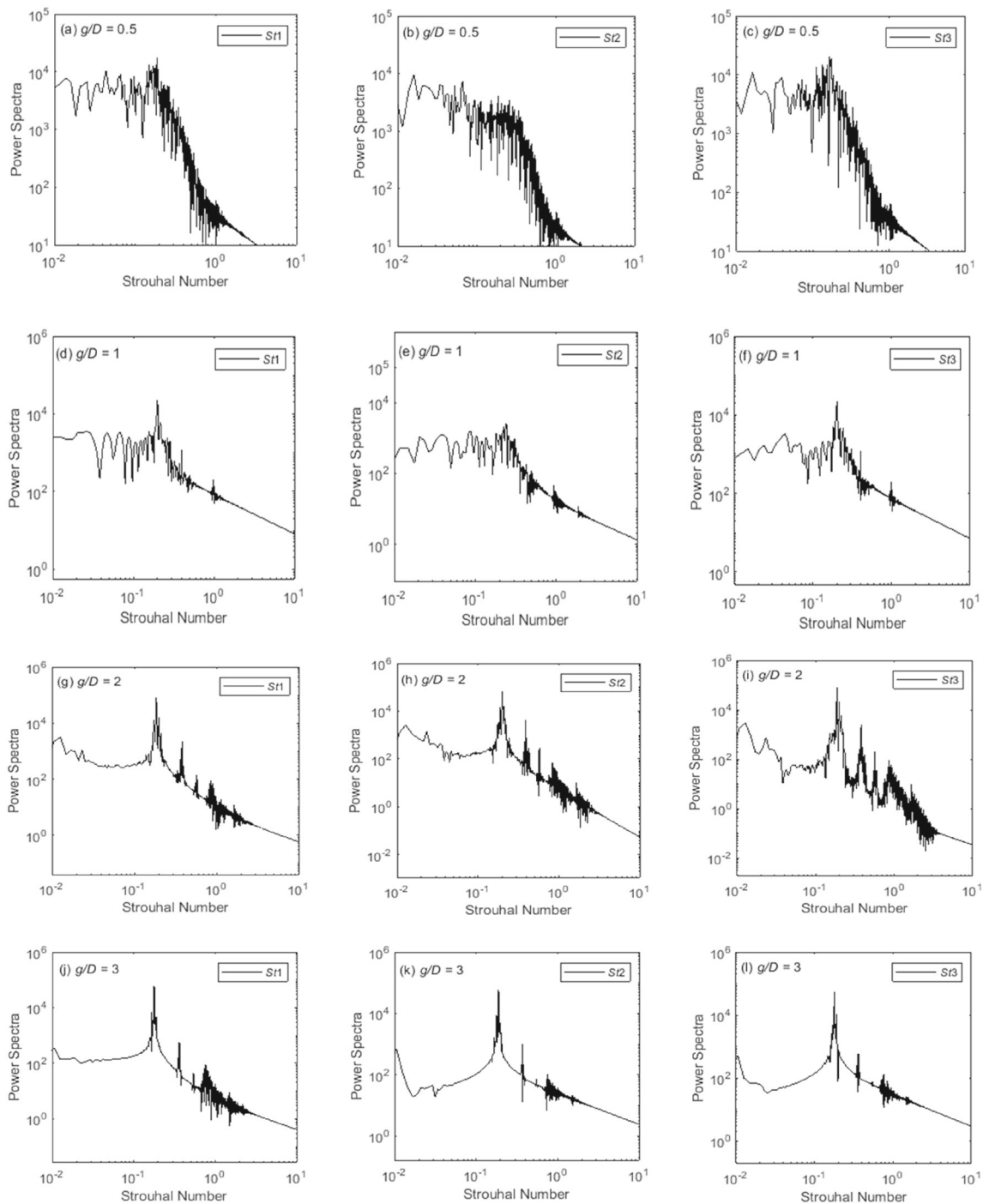
Fig. 6 (**a–i**) Spectra analysis of C_L by changing the value of g/D

coefficient of the middle cylinder (Fig. 7b). streamline visualization graph The unsteadiness is shifted more towards the middle cylinder (Fig. 4b). The amplitude of forces is also reduced as compared to $g/D = 0.5$. The difference can also be seen in terms of power spectra when varying g/D from 0.5 to 1. The less peaks in the spectra of the three structures were noted (Fig. 6d–f).

Figure 3d shows that, at relatively large spacing's ($g/D = 3$), the three cylinder wakes are fully synchronized; entailing alternate shed vortices throughout the computational domain. It can be seen that some small modulation occurs in the forces are settles to sinusoidal function (Fig. 5g, h). The power spectra investigations reveal that the three structures shed their vortices at frequencies greater than the solitary cylinder case

Fig. 7 Variation of **a** $C_{D\text{mean}}$, **b** St, **c** $C_{D\text{rms}}$, and **d** $C_{L\text{rms}}$ as a function of g/D. The dotted line represents the data of single cylinder for comparison
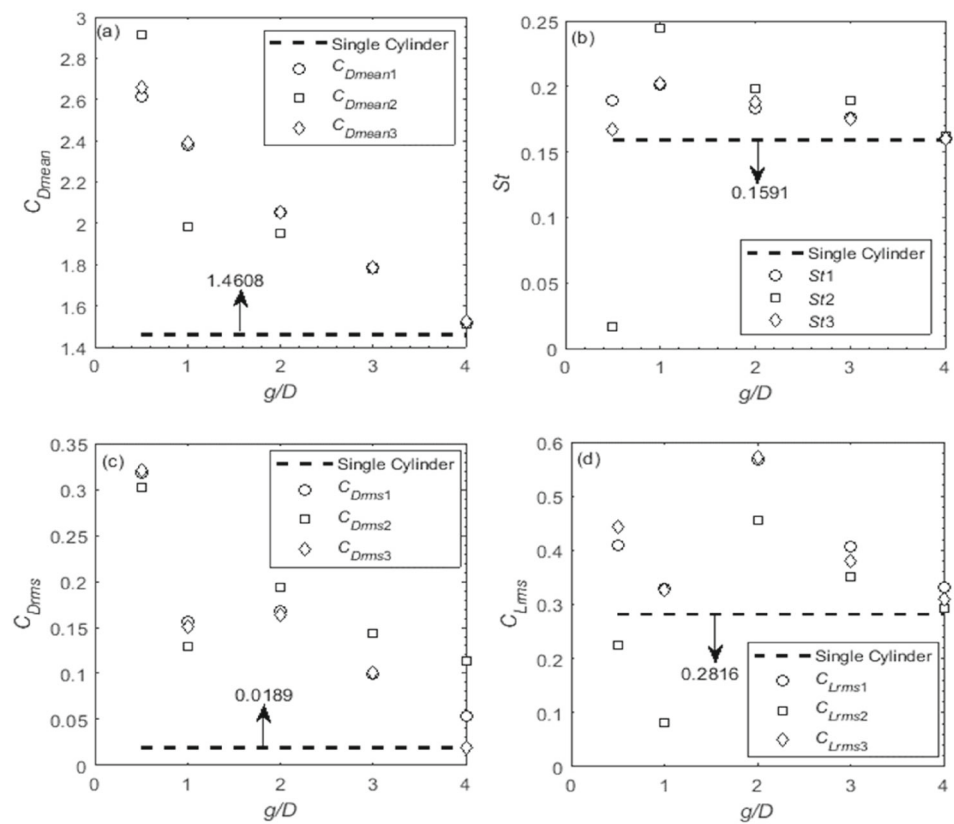
(St = 0.1591). The shedding frequency for the middle cylinder (St2 = 0.1893) is higher than the frequencies for other two cylinders (St1 = St3 = 0.1805) (see Fig. 7b). The flow regime is known as modulation-synchronized due to its slight modulation characteristics. The power spectra in Fig. 6a–i further confirms the irregular variation of forces and interaction of shed vortices. The secondary frequencies also exist together with the dominant frequency in the power spectra.

Figure 7 displays the physical parameter fluctuation for flow without splitter plates.

The variation of $C_{D\text{mean}}$ is shown Fig. 7a. The value of the $C_{D\text{mean}}$ for all the cylinders decreases with the increase in g/D values. The decreasing rate of the outer structures is very low as compared to the middle structure. At a very large value of g/D the reduction in $C_{D\text{mean}}$ for the three cylinders is almost equal to an isolated cylinder. Figure 7b shows the St variation. For the flip-flopping flow regime, the secondary frequencies dominate the flow because of the significant effect of gap flows on the wake pattern behind the cylinders. The spacing between the structures has a major impact on the frequency of vortex shedding, especially at $g/D \leq 1$. In a modulation-synchronized flow regime, the three cylinders' shedding frequencies are fairly constant, and close to those of the isolated cylinder case (St = 0.1591) at $g/D = 4$.

Figure 7c, d shows the variation of the $C_{D\text{rms}}$ and $C_{L\text{rms}}$ with g/D for Re = 150. Both $C_{D\text{rms}}$ and $C_{L\text{rms}}$ show mix

behaviour of increasing and decreasing. The $C_{D\text{rms}}$ of three cylinders is more affected as compared to mean drag coefficients (Fig. 7c). The value of $C_{D\text{rms}}$ initially start decreasing for the value of g/D up to 2 and then shows a little increase for g/D up to 3. All of the cylinders' $C_{D\text{rms}}$ values are greater than a single cylinder.

The $C_{L\text{rms}}$ of the middle structure quickly increase for the g/D where flip-flopping ($g/D = 1$) and modulation-synchronized ($g/D = 2$) flow regimes were observed (Fig. 7d). In comparison to the isolated structure ($C_{L\text{rms}} = 0.2816$) scenario, the $C_{L\text{rms}}$ of three cylinders is marginally greater.

## 5.2 Splitter plates length effect on the flow features

The gap flow effect tends to recover behind the cylinders on adopting the splitter plates with $l/D = 4$ as compared to the flow without attached splitter plates (Fig. 3a), as can be seen from the vorticity contours for $g/D = 0.5$ (Fig. 8b). The flow becomes remarkably unsteady at $g/D = 0.5$ and $l/D = 1$, as shown in Fig. 8a. This flow regime is categorized as an irregular or flip-flopping flow regime. The C_D for the middle cylinder in this flow pattern is significantly higher than the other cylinders. (Fig. 10a). The time variation of the forces shown in Fig. 10a, b indicates the irregular variation.
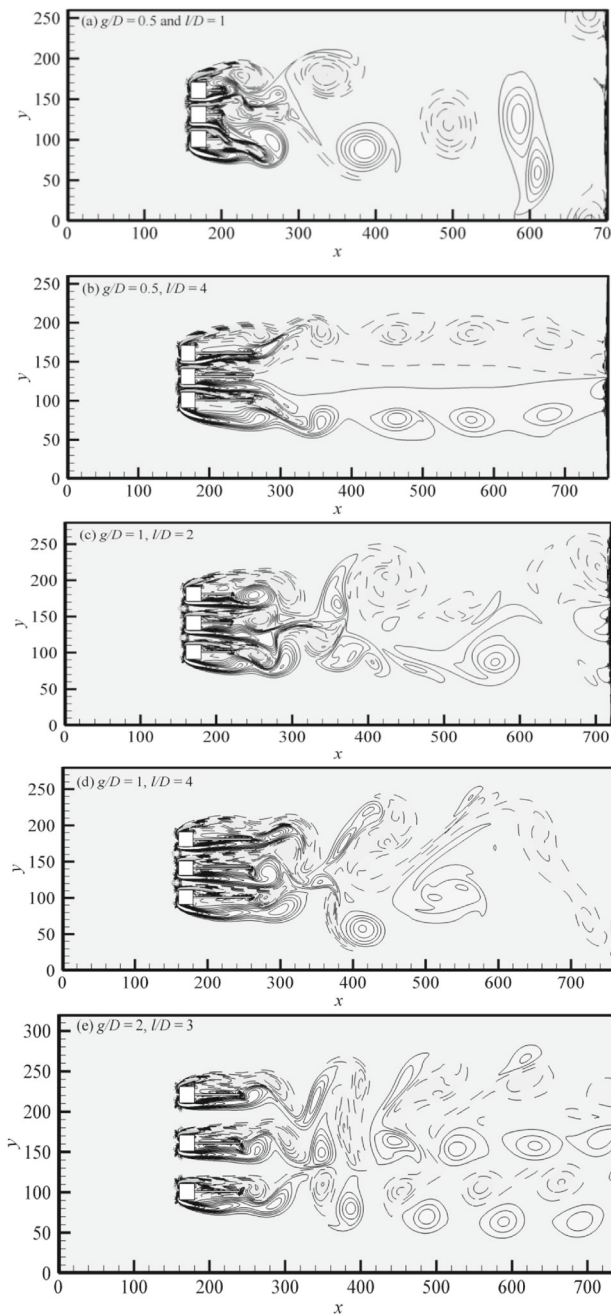
Fig. 8 (**a**–**h**) Vorticity contour visualization at different combinations of g/D and l/D

In Fig. 11a–c, the secondary structure interaction frequencies confirm the continuous toggling between the narrow and wide wakes of the outer structures as they move downstream.

With the use of splitter plates, the flow near downstream of the structures does not interact with each other, and as a result, one can see symmetric bubbles above and below the splitter surfaces in the streamline visualization graphs presented in Fig. 9a–h. At g/D = 1 with l/D = 2 and 4 in Fig. 8c, d, the flow between the cylinders after the splitter
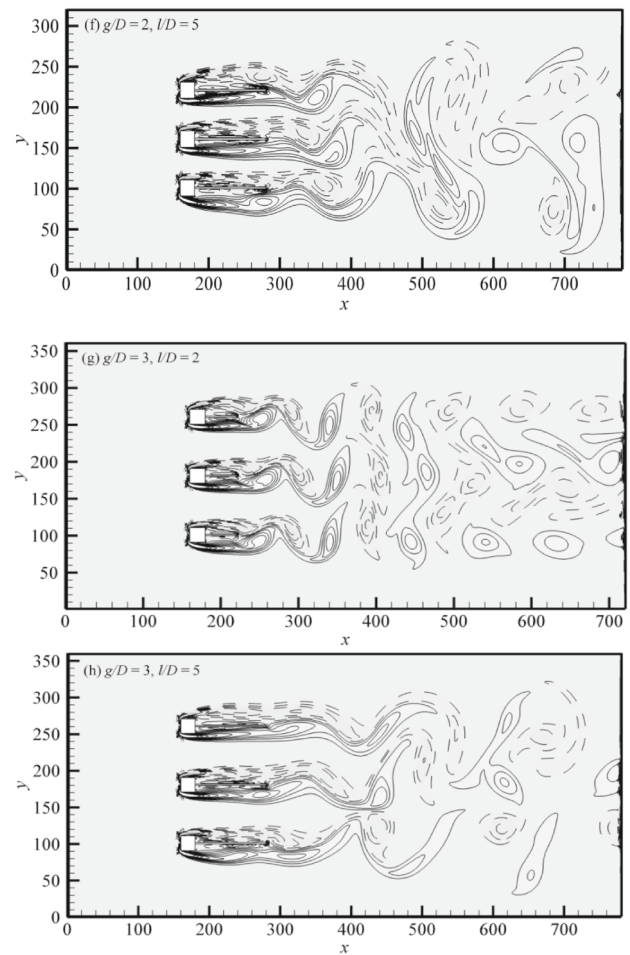
Fig. 8 continued

length deflected upwards, forming two narrow wakes behind the lower and middle structures and a wide wake behind the upper structure. Due to such deflection the time variation of C_D and C_L are completely irregular (Fig. 10e–h). This further suggests that secondary frequencies completely control the flow (see Fig. 11g–l).

The flow is completely symmetric over the splitter plates and moves independently without any serious merging as the gap between the cylinders increases (Fig. 8e). The streamlines visualization presented in Fig. 9e further confirms the independent movements of shed vortices after the splitter plates are attached to the main structures. Some modulation are observed in the time signal analysis of C_D and C_L presented in Fig. 10i, j. Increasing the splitter plates length from $l/D = 3$–5 at $g/D = 2$, the shed vortices after passing the splitter plates showed some interaction and did not move independently (Fig. 9f). The variation of C_D and C_L shows modulation behavoius for the outer cylinder (Fig. 10k, l). The spectra analysis given in Fig. 11j–l confirms the other frequencies together with the main vortex shedding frequency. As the g/D increased up to 3 (Figs. 8g, h and
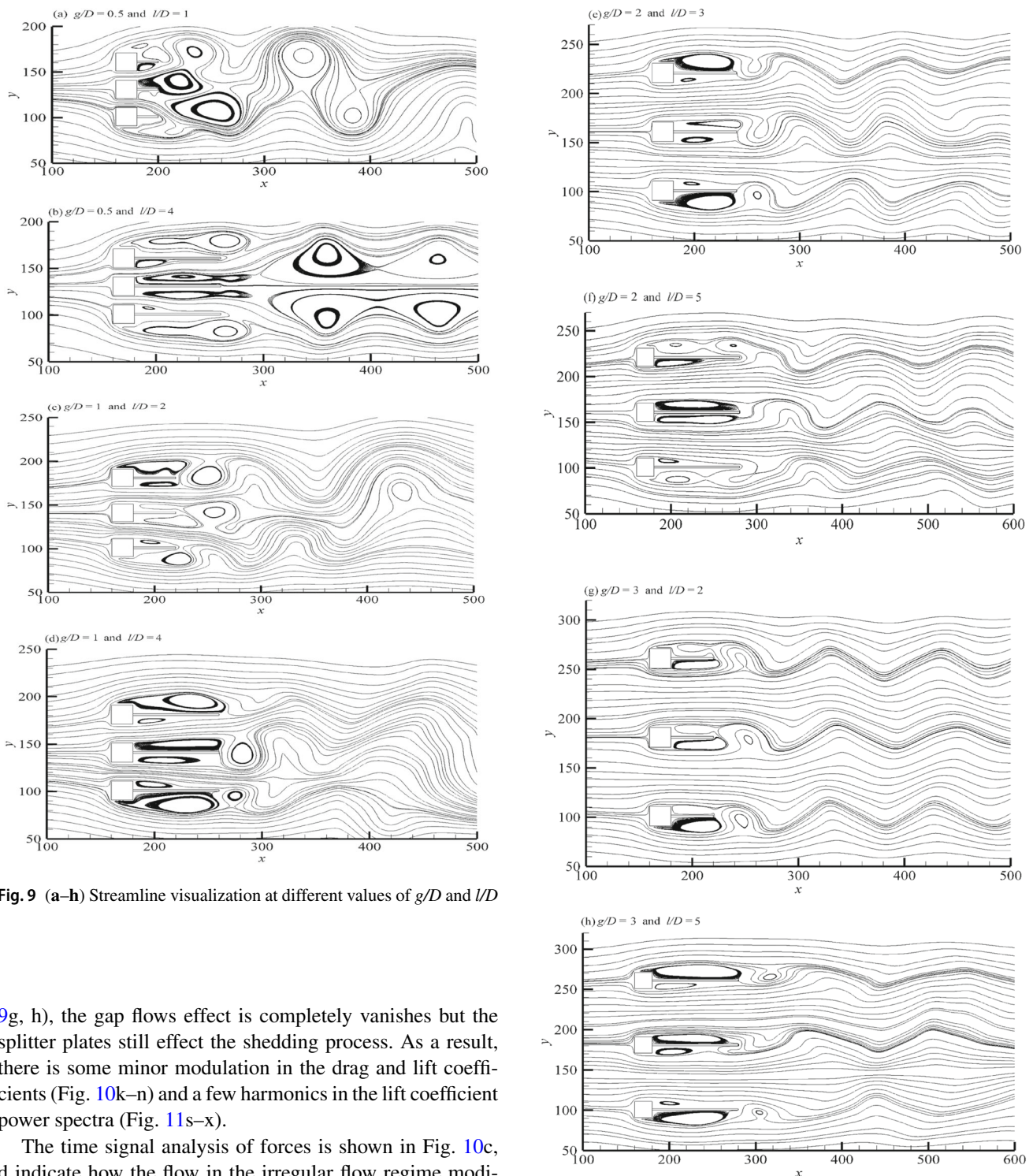
Fig. 9 (**a**–**h**) Streamline visualization at different values of *g/D* and *l/D*

Fig. 9 continued

9g, h), the gap flows effect is completely vanishes but the splitter plates still effect the shedding process. As a result, there is some minor modulation in the drag and lift coefficients (Fig. 10k–n) and a few harmonics in the lift coefficient power spectra (Fig. 11s–x).

The time signal analysis of forces is shown in Fig. 10c, d indicate how the flow in the irregular flow regime modifies and change into two-row vortex street flow regime with change of the length of the splitter plates. In case of $g/D = 1$, the three drag coefficients and lift coefficients are completely irregular without plates (Fig. 5c, d). While in the presence of splitter plates at $l/D = 4$, the three drag coefficients and lift coefficients are completely periodic without any modulation. It is to be noted that a constant drag coefficient is observed for the middle structure at $l/D = 4$.

Fig. 10 (**a**–**x**) Time variations of forces at different values of *g/D* and *l/D*
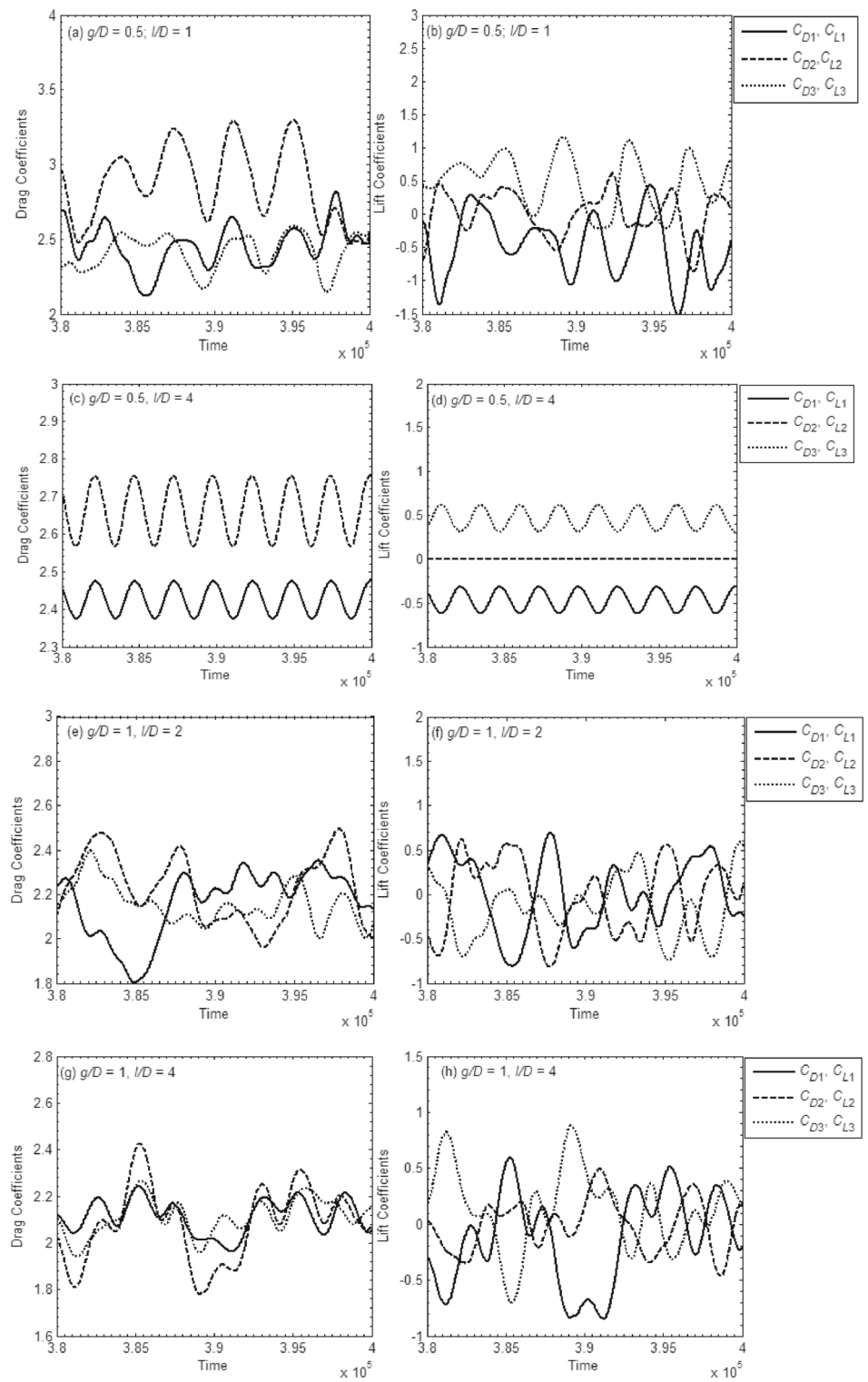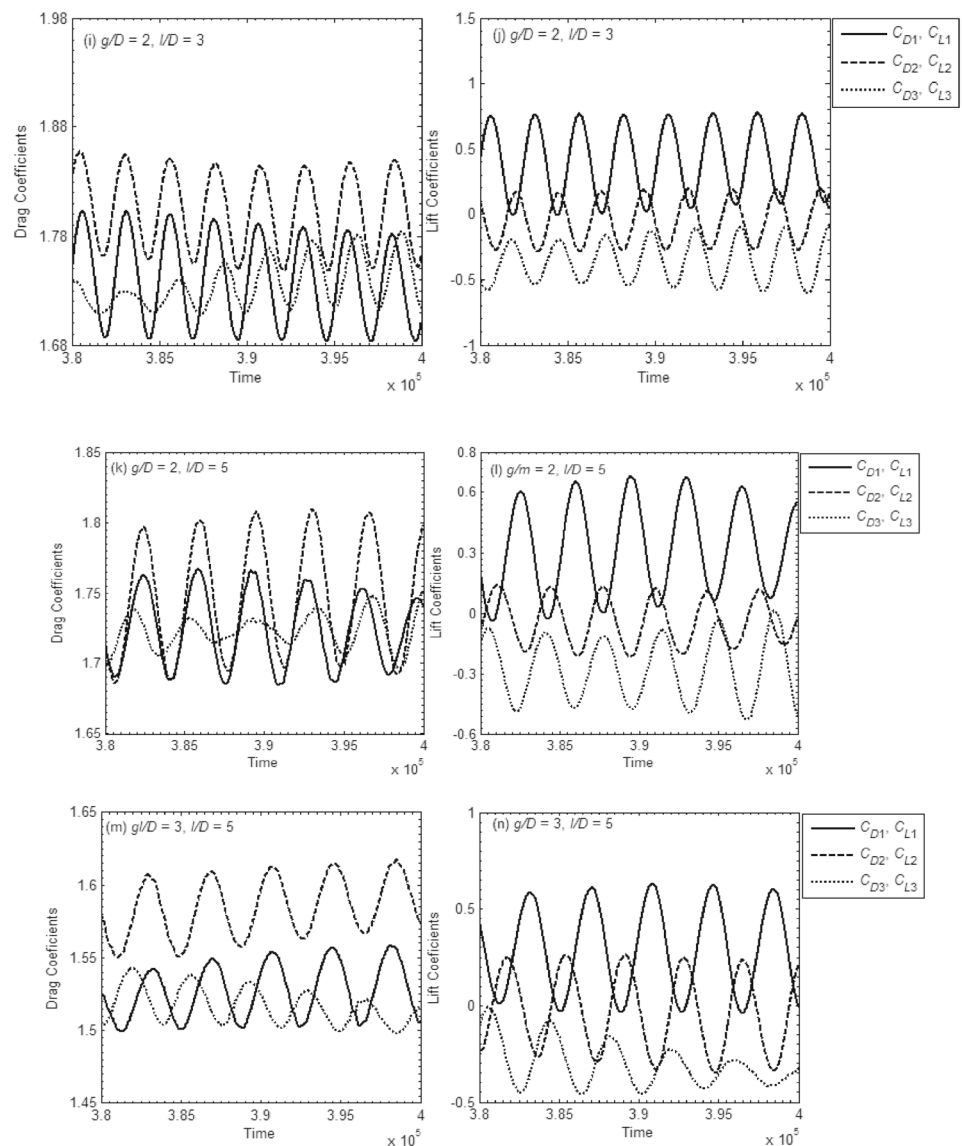
Fig. 10 continued

5.3 Force statistics

Figure 12a–e shows the fluctuation of C_{Dmean} as a function of l/D. It is observed that the C_{Dmean} of the outer cylinders decreases. At large spacing ($g/D = 4$), the C_{Dmean} of the outer cylinders becomes less than the isolated cylinder value ($C_{Dmean} = 1.4608$). As the l/D value increased, the C_{Dmean} of the middle cylinder initially decreased and subsequently marginally increased. This further reveals that at large spacing, the length of splitter plates does not strongly influence the flow parameters. This means that the adjacent wakes are practically isolated, and the wakes' interaction is minimal. The middle cylinder value is larger than the values of the outer cylinders when the flow is flip-flopping (Fig. 12a). Interestingly, the splitter plates' presence causes a drastic reduction

of the C_{Dmean} of the three cylinders at $g/D = 5$ as compared to $g/D \geq 2$.

The variation in frequency of vortex shedding as a function of l/D is shown in Fig. 13a–e. The St is found to be overly affected by strong wake interactions behind the splitter plates up to $g/D = 2$. The St decreased or increased at large spacing for all chosen cases of l/D by switching the value of l/D due to flow regime transitions. The Strouhal values of the outer cylinders are almost the same for the chosen ones. The middle cylinder is more affected as compared to the outer cylinders.

The C_{Drms} and C_{Lrms} are shown in Figs. 14a–e and 15a–e, respectively. The C_{Drms} results confirm that three cylinders are very sensitive when splitter plate length is increased. In general, the present numerical results reveal that the outer cylinders undergo large C_{Drms} as compared with the middle cylinder. It is also found that the C_{Drms} of the outer structures
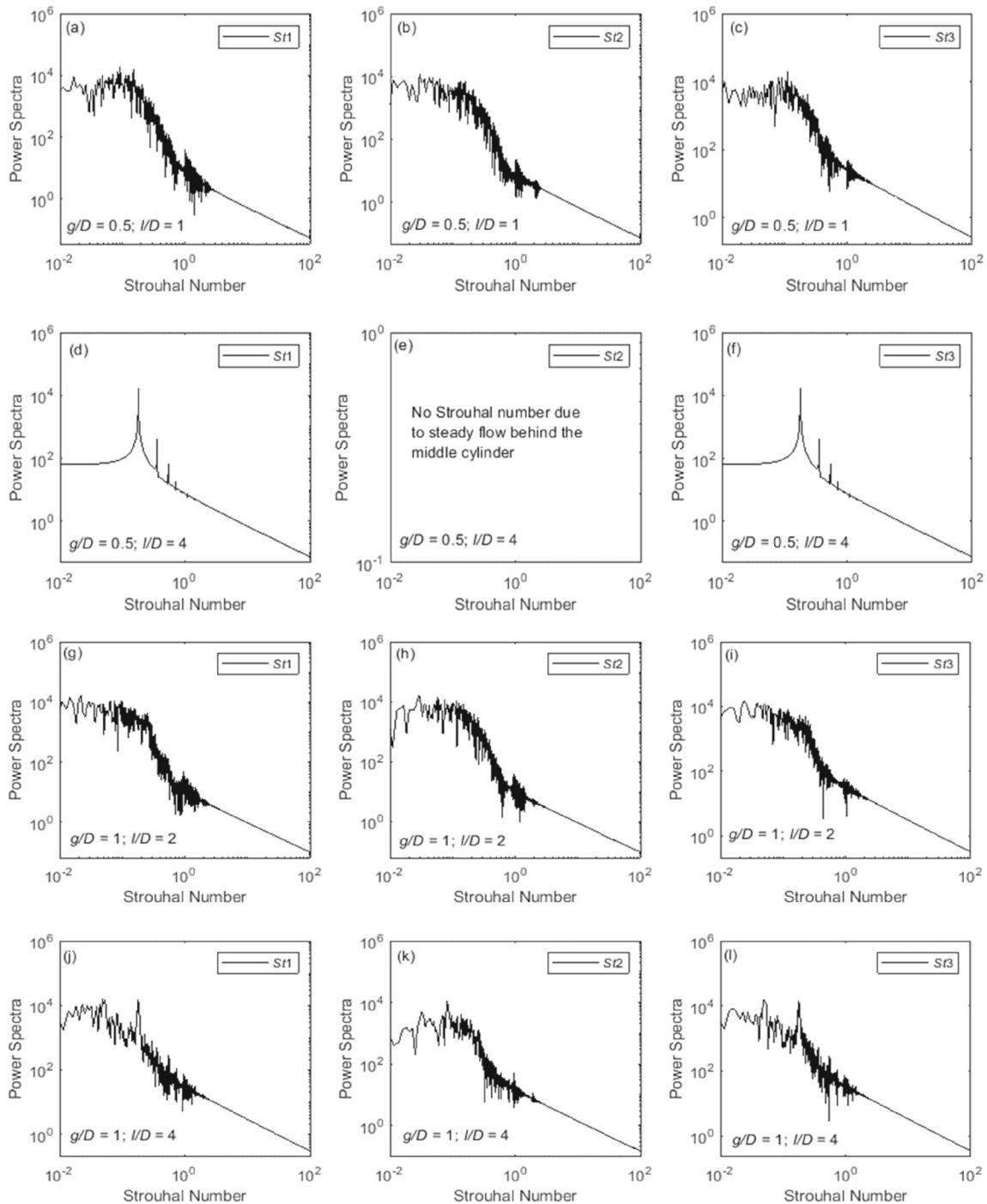
Fig. 11 (**a**–**x**). Power spectra analysis of C_L at different values of g/D and l/D

show a significant drop when l/D increases. The minimum $C_{L\text{rms}}$ for all three cylinders occur at $g/D = 0.5$ (Fig. 15a), and then are increased to the isolated square cylinder value. The findings demonstrate that the $C_{L\text{rms}}$ of the outer structures become close to the isolated structure value at $g/D = 1$ and 2. The $C_{L\text{rms}}$ of the middle cylinder is more affected as compared to the outer cylinders. The reason is that the

positive shed vortices completely stop the generation of the negative vortices generated from the upper side of the splitter plate.

Figure 16a–c shows the $C_{D\text{mean}}$ percentage reduction for the three structures at different spacing's as a function of l/D. The maximum percentage reduction is observed for the
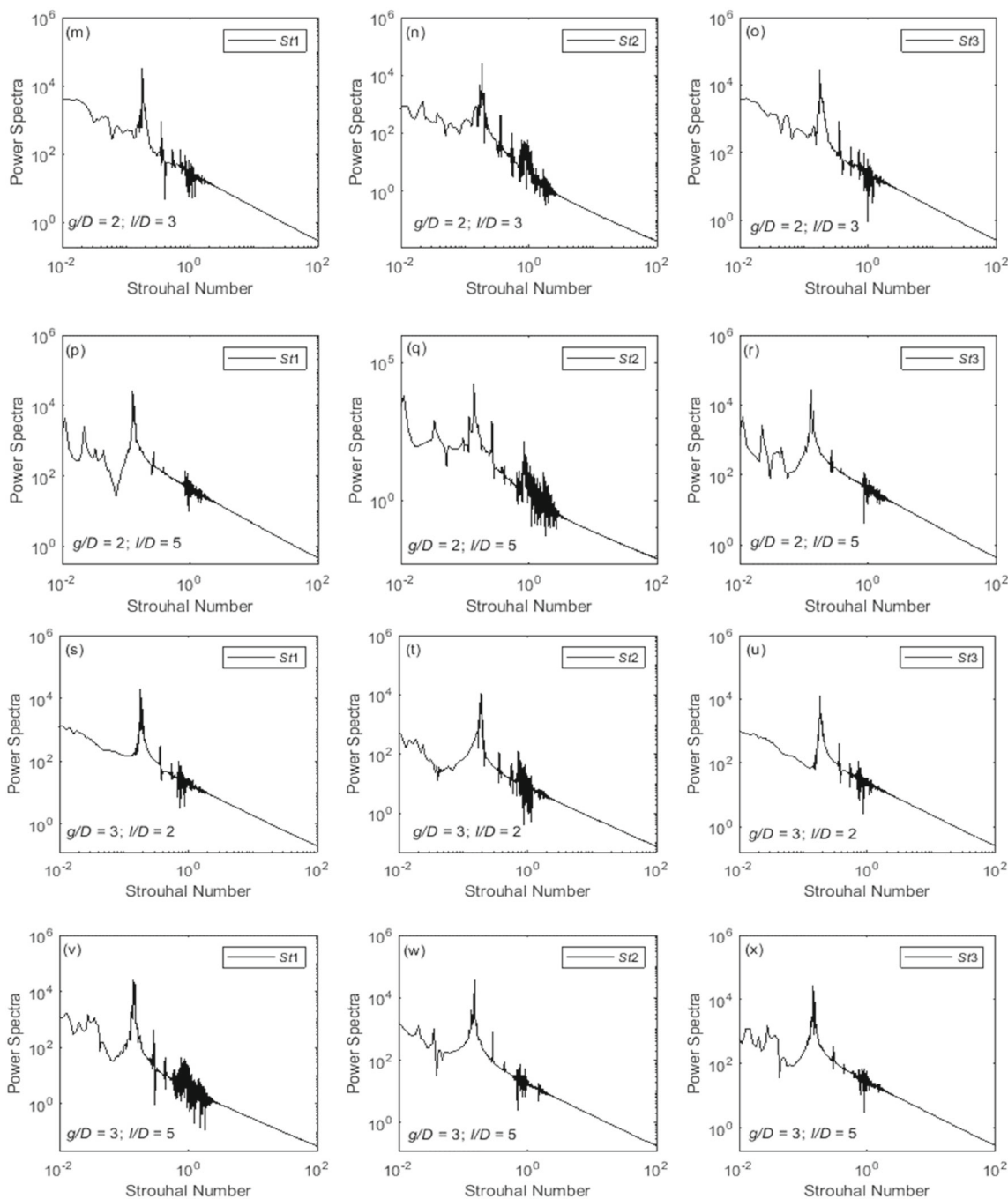
Fig. 11 continued

lower, middle, and upper cylinders at $g/D = 2$ with $l/D = 5$, $g/D = 4$ with $l/D = 0$ and $g/D = 2$ with $l/D = 5$, respectively.

6 Conclusions

This paper presents a 2D computational study for vortex shedding suppression and fluid forces reduction. The LBM was used to systematically investigate the impact of splitter plates on flow past three square cylinders placed side-by-side at Re = 150. The objective of this work was to understand the effect of separation ratio (g/D) and SP length (l/D). The combined effects of these parameters on flow were studied for $0.5 \leq g/D \leq 4$ and $1 \leq l/D \leq 5$. The main findings are:
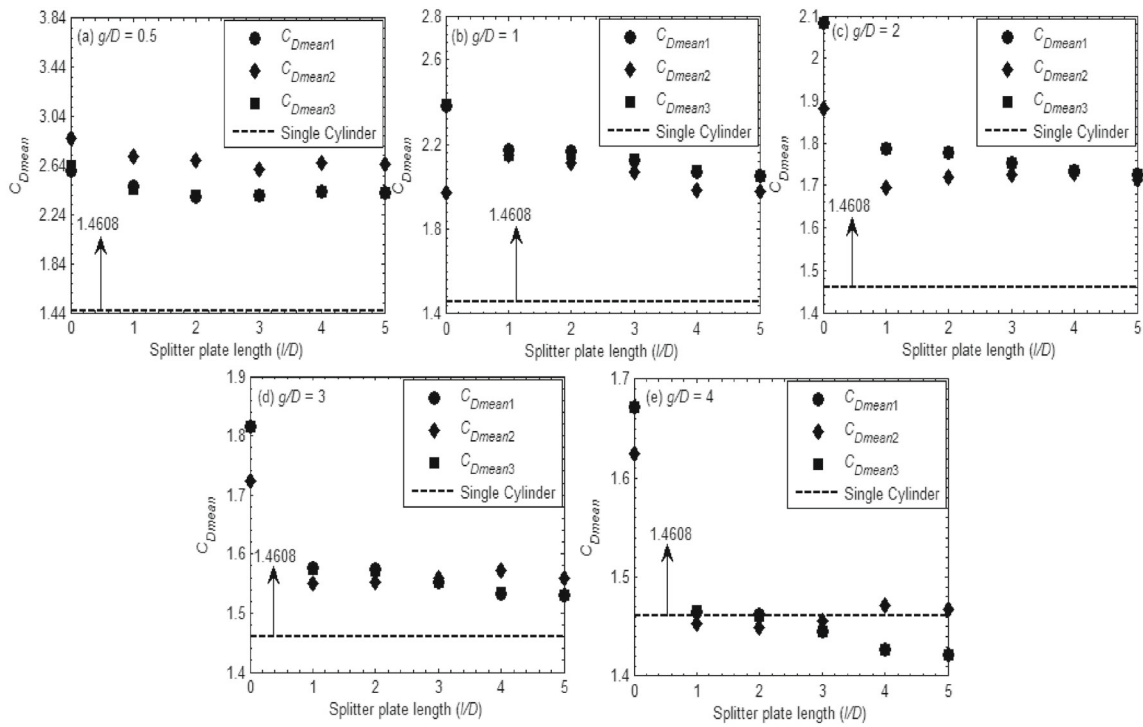
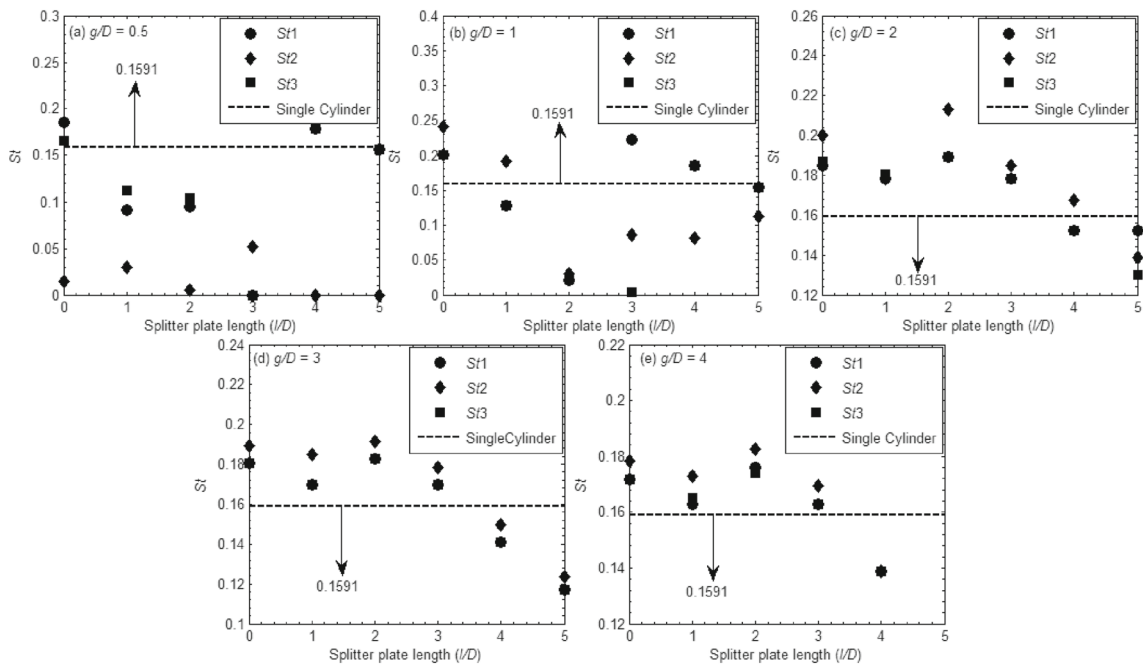**Fig. 12** (**a**–**e**) Variation of $C_{D\text{mean}}$ as a function l/D

Fig. 13 (**a**–**e**) Variation of St as a function of l/D
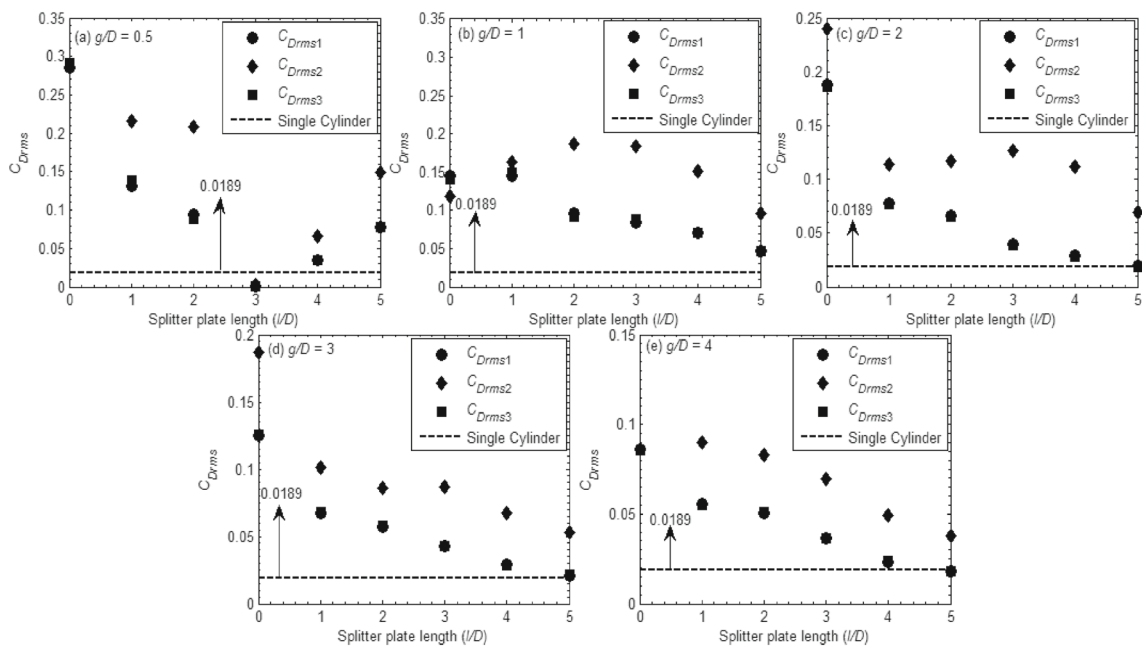
Fig. 14 (**a–e**) Variation of $C_{D\mathrm{rms}}$ as a function of l/D
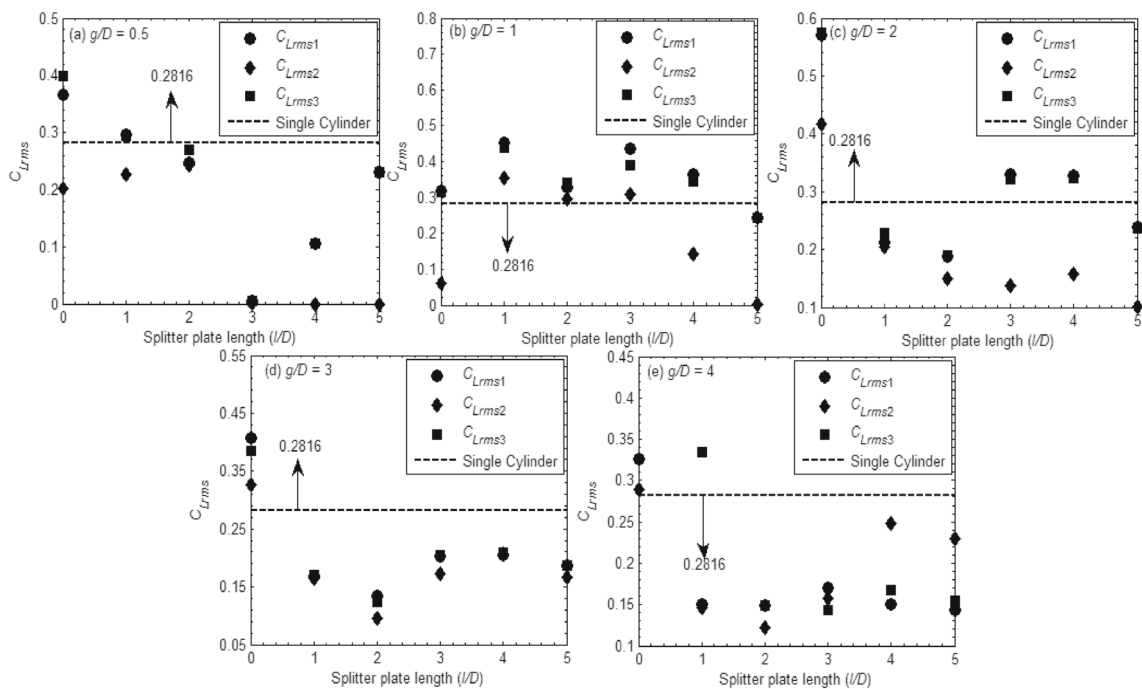

Fig. 15 Variation of $C_{L\mathrm{rms}}$ as a function of l/D

I. Five different flow patterns have been observed, namely; deflected; flip-flopping; symmetric; inphase-antiphase synchronized and inphase synchronized flow patterns.

II. At very small spacing the vortices are completely chaotic and showing merging behaviour due to jet interaction. The splitter plates play a vital role to suppress the shedding and reduced the drag on the objects.

III. The splitter with the larger length fully controls the jet interaction at low spacing values. In the presence of long splitter plates ($l/D = 4$) behind the cylinders at
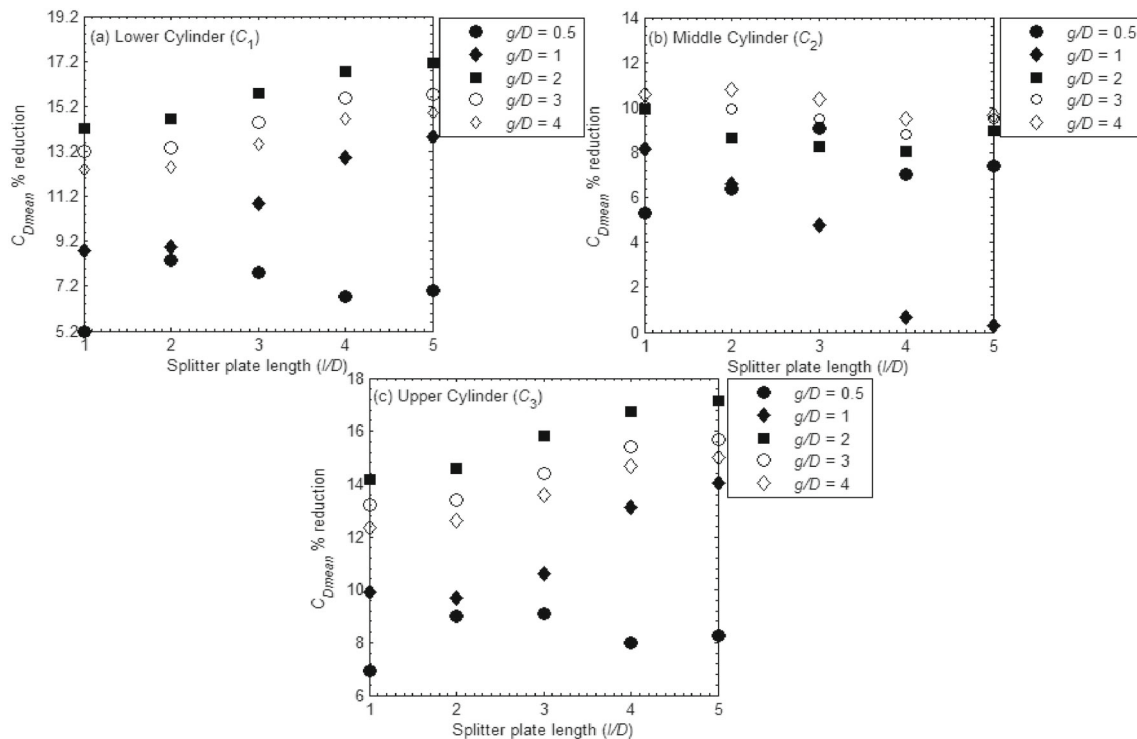
Fig. 16 (**a**–**c**) Percentage $C_{D\text{mean}}$ of flow past three cylinders as a function of l/D

$g/D = 0.5$, the three structures C_D are periodic, and the flow transition occurs from irregular flow to a two-row vortex street flow regime. The irregular or flip-flopping flow regime was also observed by Kang [19] for low Re. The power spectra for this flow regime demonstrates how separate dominant frequencies are randomly spread over a particular range.

IV. The shedding frequency greatly varies on the g/D, especially at $g/D \leq 1$. In case of modulation-synchronized flow regime, the three cylinders' shedding frequencies are nearly constant, and very similar to the isolated cylinder case (St = 0.1591) at $g/D = 4$.

V. The shedding frequency of the middle cylinder attains its minimum value at $g/D = 0.5$, and then attains its maximum value at $g/D = 1$. This is due to the unsteadiness shifting toward the middle structure.

VI. The C_D and C_L signals completely followed the pattern observed in the vorticity contour visualization graphs. The maximum reduction in $C_{D\text{mean}}$ is observed for the lower and upper structures at $(g/D, l/D) = (1, 5)$, that is, 20%, where the flow mode is symmetric. There is 100% reduction in St for the middle structure at $(g/D, l/D) = (0.5, 5)$.

References

1. Gad-el-Hak M (2000) Flow control, passive, active and reactive management. Cambr Univ Press 11:17–26
2. Choi H, Jeonand WP, Kim J (2008) Control of flow over a bluff body. Ann Rev Fluid Mech 40:113–139
3. Roshko A (1954) On the drag and shedding frequency of two-dimensional bluff bodies NACA Technical Note 3169
4. Wu J, Shu C (2011) Numerical study of flow characteristics behind a stationary circular cylinder with a flapping plate. Phys Fluids 17(1):0736015
5. Okajima A, Nakamura A, Kosugi T, Uchida H, Tamaki R (2004) Flow-induced in-line oscillation of a circular cylinder. Eur J Mech B Fluids 23(1):115–125
6. Doolan CJ (2009) Flat-plate interaction with the near wake of a square cylinder. AIAA J 47:475
7. Chauhan MK, Dutta S, More BS (2018) Experimental investigation of flow over a square cylinder with an attach splitter plate at intermediate Reynolds number. J Fluids Struct 76:319–335
8. Hwang J, Yang K (2008) Drag reduction on a circular cylinder using dual detached splitter plates. J Wind Eng Ind Aerodyn 95:551–564
9. Vamsee GR, Tenae ML, Tiwari S (2014) Effect of arrangement of inline splitter plate on flow past square cylinder. Prog Comput FluidDyn Int J 14:277–294
10. Ul Islam S, Manzoor R, Zhou CY, Rashdi MM, Khan A (2017) Numerical investigation of fluid flow past a square cylinder using upstream, downstream and dual splitter plates. J Mech Sci Technol 31:669–687
11. Ali MS, Doolan CJ, Wheatley V (2011) The sound generated by a square cylinder with a splitter plate at low Reynolds number. J Sound Vib 330:3620–3635
12. Cete AR, Unal MF (1992) Effects of splitter plate on wake formation a circular cylinder: a discrete vortex simulation. Comput Fluid Dyn 1:349–356

13. Kim HJ, Durbin PA (1988) Investigation of the flow between a pair of circular cylinders in the flopping regime. J Fluid Mech 196:431–448

14. Furquan M, Mittal S (2015) Flow past two square cylinders with flexible splitter plates. Comput Mech 55:1155–1166

15. Ahmed A, Islam SU, Zhou CY, Manzoor R (2020) Fluid dynamics around three inline cylinders in presence of small control cylinders. Can J Phys 98(11):1060–1076

16. Zhang HJ, Zhou Y (2001) Effect of unequal cylinder spacing on vortex streets behind three side-by-side cylinders. Phys Fluids 13(12):3675–3686

17. Virahsawmy HK, Chen L, MacGillivray IR, Tu J, Zhou Y (2005) Computation of flow behind three side-by-side cylinders of unequal/equal spacing. ANZIAM J 46:672–989

18. Junkao L, Yaqiang H, Dibo D, Weisha C (2016) Flow features of three side-by-side circular cylinders at low Reynolds number. ICMMR 77:04007

19. Kang S (2004) Numerical study on laminar flow over three side-by-side cylinders. KSME Int J 18(10):1869–1879

20. Sumner D, Wong SST, Price SJ, Paidoussis MP (1999) Fluid behavior of side-by-side circular cylinders in steady cross-flow. J Fluids Struct 13:309–339

21. Rahman H, Islam SU, Abbasi WS, Nazeer G (2020) A numerical study for flow around three square cylinders in triangular arrangement. Iran J Sci Technol Trans Mech Eng 44:229–246

22. Zheng Q, Alam MM (2017) Intrinsic features of flow past three square prisms in side-by-side arrangement. J Fluid Mech 826:996–1033

23. Ul Islam S, Rahman H, Ying ZC (2016) Comparison of wake structures and force measurements behind three side-by-side cylinders. J Braz Soc Mech Sci 38:843–858

24. Inoue O, Suzuki Y (2007) Beat of sound generated by flow past three side-by-side square cylinders. Phys Fluids 19(4):048102

25. Kumada M, Hiwada M, Ito M, Mabuchi I (1984) Wake interference between three circular cylinders arranged side by side normal to a flow. Trans JSME 50:1699–1707

26. Guillaume DW, LaRue JC (1999) Investigation of the flopping regime with two-three- and four-cylinder arrays. Exp Fluids 27:145–156

27. Zafar ZUA, Zaib S, Hussain MT, Tunç C, Javeed S (2022) Analysis and numerical simulation of tuberculosis model using different fractional derivatives. Chaos Solitons Fractals 160:112202

28. Khan H, Ahmad F, Tunç O, Idrees M (2022) On fractal-fractional Covid-19 mathematical model. Chaos Solitons Fractals 157:111937

29. Zafar ZUZ, Samina Y, Sumera Z, Tunç C (2022) An efficient numerical simulation and mathematical modeling for the prevention of tuberculosis. Int J Biomath 15(04):2250015

30. Guo Z, Liu H, Luo LS, Xu K (2008) A comparative study of the LBE and GKS methods for 2D near incompressible laminar flows. J Comput Phys 227(10):4955–4976

31. Zhou CY, Wang L, Huang W (2009) Numerical study of fluid force reduction on a circular cylinder using tripping rods. J Mech Sci Tech 21:1425–1435

32. Yu D, Mei R, Luo LS, Shyy W (2003) Viscous flow computations with the method of lattice Boltzmann equation. Prog Aerosp Sci 39(5):329–367

33. Frisch U, Hasslacher B, Pomeau Y (1986) Lattice gas automata for the Navier–Stokes euations. Phys Rev Lett 56:1505–1508

34. Breuer M, Bernsdorf J, Zeiser T, Durst F (2000) Accurate computations of the laminar flow past a square cylinder based on two different methods: lattice-Boltzmann and finite-volume. Int J Heat Fluid Flow 21(2):186–196

35. Okajima A (1982) Strouhal numbers of rectangular cylinders. J Fluid Mech 123:379–398

36. Sohankar A, Norberg C, Dvidson L (1997) Numerical simulation of unsteady low-Reynolds number flow around rectangular cylinders at incidence. J Wind Eng Ind Aerodyn 69:189–201

37. Gera B, Sharma PK, Singh RK (2010) CFD analysis of 2D unsteady flow around a square cylinder. Int J Appl Eng Res 1(3):602–610